Stochastic Periodic Microstructures for Multiscale Modelling of Heterogeneous Materials

Evan John Ricketts[1] (ID)

© The Author(s) 2024

Abstract

Plurigaussian simulation is a method of discrete random field generation that can be used to generate many complex geometries depicting real world structures. Whilst it is commonly applied at larger scales to represent geological phenomena, the highly flexible approach is suitable for generating structures at all scales. Here, an extension of plurigaussian simulation to periodic plurigaussian simulation (P-PGS) is presented, such that the resulting fields are periodic in nature. By using periodic Gaussian random fields as components of the method, periodicity is enforced in the generated structures. To substantiate the use of P-PGS in capturing complex heterogeneities in a physically meaningful way, the pore-scale microstructure of cement paste was represented such that its effective properties can be calculated through a computational homogenisation approach. The finite element method is employed to model the diffusion of heat through the medium under dry and saturated pore conditions, where numerical homogenisation is conducted to calculate the effective thermal conductivity of the medium. Comparison of the calculated values with experimental observations indicated that the generated microstructures are suitable for pore-scale representation, given their close match. A maximal error of 1.38% was observed in relation to the numerically determined effective thermal conductivity of mortar paste with air filled pores, and 0.41% when considering water filled pores. As the assumption of a periodic domain is often an underlying feature of numerical homogenisation, this extension of plurigaussian simulation enables a path for its integration into such computational schemes.

Article Highlights

- Integrating P-PGS into numerical homogenisation frameworks enhances complex heterogeneous material representation
- The flexibility of P-PGS enables a wide range of material microstructures to be represented accurately
- Use of the generated structures allows material properties to be estimated accurately through numerical homogenisation

---

✉ Evan John Ricketts
  rickettse1@cardiff.ac.uk

[1] School of Engineering, Cardiff University, Cardiff CF24 3AA, UK

1 Introduction

Understanding the complex response of materials at different scales can give insight into
their overall behaviour, where often the micro-level dynamics have a large influence on
the macro-level response. This is true for many mechanical or transport-based processes,
which are often dependent on the geometry of the discrete structures seen at each level.
One such process is thermal diffusion, where the thermal conductivity is a key considera-
tion when employing materials in the built environment. For example, insulative proper-
ties of materials can significantly influence comfort and heating costs for individuals in
surrounding areas. Similarly, it has been shown that the associated damage mechanisms
of these heterogeneous materials originates from thermal-related micro- and meso-scale
behaviour (Evans 1978), highlighting the need for accurate prediction at all scales of obser-
vation of effective material properties.

In the first instance, research focussed on the behaviour of heterogeneous solids through
variational principles, such that upper and lower bounds could be computed for the effec-
tive material properties (Rosen and Hashin 1970; Hashin 1983; Gibiansky and Torquato
1997). An alternative approach was then taken, deriving closed-form expressions for said
properties based on a solution of inclusions within an infinite medium (Noor and Shah
1993), but often relied on idealisation of the material geometry and system response. The
use of asymptotic methods has been considered for determining the constitutive compo-
nents of periodic microstructures (Auriault 1983). Originally being used to solve differ-
ential equations with periodic boundary conditions, the approach utilises an asymptotic
expansion of a given unknown field such as temperature or displacement, and truncates
the higher-order terms to give homogenised properties. Due to the significant advancement
of computational resources, many approaches have been developed for numerical homog-
enisation (Ghosh and Liu 1995; Jiang et al. 2002), often using the finite element method
(FEM) in conjunction with multi-level simulation (Özdemir et al. 2008; Rocha et al. 2021;
Ricketts et al. 2023c). Macro-level models are fed information about the solution -calcu-
lated at various scales- such that the need for highly empirical relations is negated, and
is seen in methods such as FE^2 (Feyel and Chaboche 2000) and equation free modelling
(Bindal et al. 2006; Tretiak et al. 2022). Typically, these are computationally expensive,
as a boundary value problem (BVP) is solved at the micro-scale for each integration point
in the macro-level domain. It is worth noting that methods have been developed to reduce
this cost, such as neural network based surrogate models (Lefik et al. 2009; Ghavamian and
Simone 2019; Rocha et al. 2020), and model order reduction techniques (Chaturantabut
and Sorensen 2010; Kerfriden et al. 2011; Goury et al. 2016; Ghavamian et al. 2017).

The unifying factor in all the considered approaches is that a description of the micro-
scale geometry is necessary in terms of a representative volume element, over which the
homogenisation process is conducted. Generally, this is simplified in terms of the geom-
etry, and is often not representative of the true complex microstructural geometry, which
is known to impact the resulting effective properties. Whilst experimentally obtained scans
-e.g. from micro-X-ray computed tomography- could be used as the BVP domain, these are
often expensive to analyse in terms of time and computing resources (Le Houx et al. 2023).
It would be advantageous to be able to generate these virtually at low computational cost.

Many methods exist for generating virtual cementitious materials, such as the use of CEM-HYD3D (Bentz 2006), aggregate placing methods (Zhang et al. 2018; Thilakarathna et al. 2020; Holla et al. 2021), machine learning alternatives (Cruz et al. 2016), with the most commonly used being HYMOSTRUC3D (van Breugel 1995; Patel et al. 2018a).

Plurigaussian simulation (PGS) is a lesser explored stochastic method for microstructural generation. It was first introduced by Galli et al. (1994), and developed further in the following years (Loc'h and Galli 1997; Dowd et al. 2003; Armstrong et al. 2014) for geological applications. The method is based on the truncation of Gaussian random fields (Matheron et al. 1987; Beucher and Renard 2016), but unlike the sequential relationship that the resulting field has between its phases, PGS can produce more complex connectivity between its phases in a non-sequential manner. This is determined by a prescribed lithotype rule, which controls the distinct geometry and proportions of the generated field, as well as the spatial relationship between facies (Doligez et al. 2011). The method commonly applied in representing field scale structures such as ore deposits or geologic formations (Betzhold and Roth 2000; Yunsel and Ersoy 2011; Renard and Beucher 2012; Talebi et al. 2013; Maleki and Emery 2014; Mery et al. 2017; Teles et al. 2023) and petroleum reservoirs (Chautru et al. 2015; Beucher and Renard 2016; Zagayevskiy and Deutsch 2016; Martinius et al. 2017; Madani et al. 2018), but has also been used at much smaller scales such as in the generation of the micro-structure of solid oxide cells (Abdallah et al. 2016), porous media (Méndez-Venegas and Díaz-Viera 2013), mineral microstructures (Teichmann et al. 2021), as well as concrete at various scales for the calculation of effective diffusion coefficients through a multi-level approach (Ricketts et al. 2023c).

In many asymptotic or computational homogenisation approaches, the micro-scale representative volume elements are assumed periodic. Thus, in this study, the PGS framework is extended to allow for the generation of periodic structures, being denoted as P-PGS. The highly flexible approach allows for the generation of many complex discrete geometries with minimal computational cost. A series of pore-scale representations of cement paste are generated based on experimental observations (Khan 2002; Liu et al. 2020; Stolarska and Strzałkowski 2020), and their effective thermal conductivities are calculated for dry and saturated pore conditions. Finally, these are compared against experimental values to assess the generated microstructures in being representative of the pore-scale geometry. Taking a numerical approach for material characterisation allows for a much wider description of the material to be attained much more quickly than the equivalent experimental process. The use of P-PGS enables the quantification of material properties based on a more closely fitting geometric representation than current solutions offer, such as pore network modelling (Van Marcke et al. 2010; Yang et al. 2019).

Here, the simulations are conducted in 2D, but it is noted that there is an intrinsic difference between 2D analyses and the 3D reality of pore-scale transport processes, being inherently three dimensional. Despite the potential for discrepancy in qualitative information, 2D representations have been employed as a step towards more complex 3D investigations, where this methodological choice is rooted in the current scope of the research. As will be seen in Sect. 4, the results correlate well with experimental data for thermal conductivity under both dry and saturated conditions, validating the robustness and relevance of the 2D approach within its acknowledged limitations. Whilst 3D analyses hold the promise of yielding quantitatively differing results, the approach is conceptually equivalent in 2D, and provides a basis for understanding transport phenomena at the pore-scale.

The layout for the remainder of the paper is as follows: Sect. 2 presents the theory of the PGS model, its extension to P-PGS, and the numerical homogenisation regime that is

employed; Sect. 3 gives the numerical formulation of the finite element solution for heat transport through Poisson's equation, as well as numerical details of the field generation; Sect. 4 presents the determination of the effective thermal conductivity for cement paste; and Sect. 5 highlights the main conclusions of the study.

2 Theoretical Basis

In the following, the PGS theory and the chosen numerical homogenisation scheme are given. The applied numerical approach will allow the effective thermal conductivity of cement paste to be calculated under steady state conditions. It is worth noting that this can also be done for the transient case, as well as for other material properties, but these will not be considered here. The method is versatile, suitable for thermal properties across various materials, and will be presented with this generality in mind. Similarly, the formulation relating to PGS and its periodic extension will be presented in $\mathbb{R}^2$. Whilst the method is not limited by dimensionality -being equally as applicable in $\mathbb{R}^3$, for instance- the cases that will be considered in later sections are in $\mathbb{R}^2$, hence, the formulation will be given in this space for consistency.

2.1 Periodic Plurigaussian Simulation

Let $\{Z_1, Z_2\}$ be a set of two independent random fields in $\mathbb{R}^2$, such that the random field $\mathbf{Z}$ is defined as

$$\mathbf{Z}(\boldsymbol{x}) = \big(Z_1(\boldsymbol{x}), Z_2(\boldsymbol{x})\big), \forall \boldsymbol{x} \in \mathbb{R}^2 \tag{1}$$

Then, let $L = \{D_1, \dots, D_n\}$ be a partition of $\mathbb{R}^2$ into n disjoint subdomains, such that the resulting random field $\mathbf{P}$ with at most n distinct facies is defined as

$$\mathbf{P}(\boldsymbol{x}) = i \Leftrightarrow \mathbf{Z}(\boldsymbol{x}) \in D_i, \forall \boldsymbol{x} \in \mathbb{R}^2 \tag{2}$$

where i is the phase of D_i. The set L is the lithotype rule, and determines the number phases that could be present in the resulting field $\mathbf{P}$, where each phase is related to a facie D_i. Figure 1d presents an example realisation of that is generated through PGS, where the random fields have a Gaussian kernel (a, b), and L consists of 3 quadrilateral facies (c).

The covariance structure of the random fields Z_1, Z_2 influences the general form of $\mathbf{P}$, where here the smoothness of (a, b) result in a smooth field (d). Using a rougher covariance structure, such as the Matérn kernel, will result in a rougher realisation of $\mathbf{P}$ (Ricketts et al. 2023c). The lithotype also allows control of the connectivity between phases in $\mathbf{P}$. If two facies are not connected in L, then the same will be true in $\mathbf{P}$. This allows for complex structures to be represented based on careful choices of L.

Similarly, to the use of non-stationary random fields in generating a non-stationary field of $\mathbf{P}$, the extension to P-PGS relies on the generated fields Z_1, Z_2 being periodic. For both Z_1 and Z_2, their values on opposing boundaries will be equal, such that they map to the same position in L. If the generated random fields are now assumed periodic, denoted as $\overline{Z_1}$, $\overline{Z_2}$, the convolutional nature of the method ensures that the periodicity of $\overline{Z_1}$, $\overline{Z_2}$ enforces periodicity in $\mathbf{P}$. This is illustrated in Fig. 2, where (a) depicts a more complex

Fig. 1 Schematic of plurigaussian simulation where **a**, **b** are gaussian random fields, **c** is the lithotype rule consisting of 3 facies, and **d** is the resulting simulated field **P**
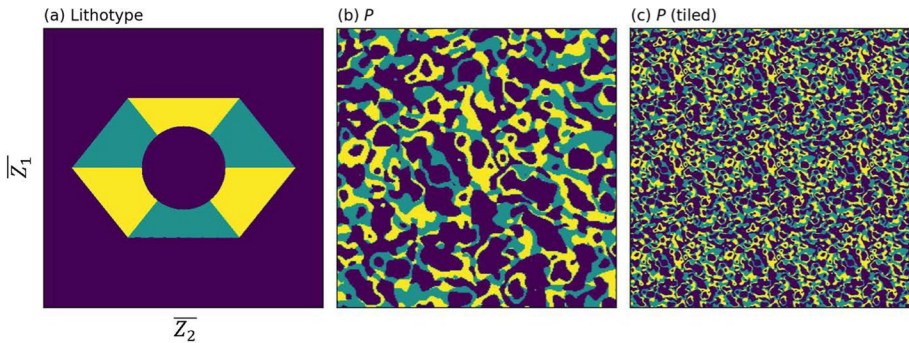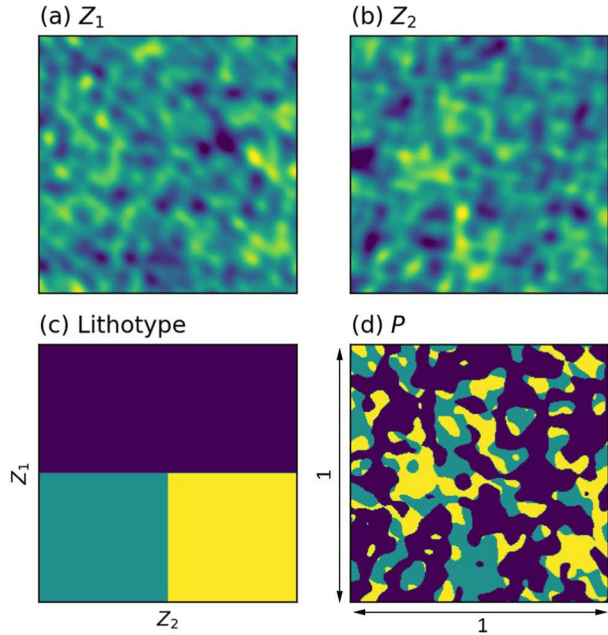
(a) Z_1

(b) Z_2

(c) Lithotype

(d) P

Fig. 2 An example of P-PGS where **a** is the lithotype rule, **b** is the resulting periodic field **P**, and **c** is a tiled illustration of **P** to highlight its periodicity

lithotype rule, (b) gives the resulting field **P**, and (c) illustrates a tiled version of **P** to shows its periodicity.

The extension to P-PGS was inspired by numerical homogenisation techniques. In many cases, the calculation of effective material properties is done numerically over domains which mimic the structures found at different levels of the material. Often, the microstructure of composite materials is assumed periodic in numerical homogenisation approaches (Andreassen and Andreasen 2014), hence, extending to P-PGS allows for greater flexibility in the usage of the generated structures, making it highly appropriate for multi-level material representation.

2.1.1 Random Field Generation

Random fields are a key component of PGS, where the covariance kernel of the input fields will dictate the characteristics of the resulting discrete field (Ricketts et al. 2023c). Gaussian random fields are a common choice due to their smooth behaviour making them suitable at representing many spatially varying parameters. Various methods exist to generate such fields, with the choice often being dictated by the computational efficiency of the method. Covariance matrix decomposition (CMD) is commonly adopted due to its simplicity and accuracy, in which a random field $\mathbf{Z}$ can be computed as $\mathbf{Z} = \mathbf{LN}$, where $\mathbf{N}$ is a vector sampled from a standard normal distribution, $\mathbf{L}$ is the decomposition matrix satisfying $\mathbf{LL}^T = A$, and A is the correlation matrix for all locations (Li et al. 2019). Cholesky- or eigen-decomposition is often used in the computation of $\mathbf{L}$, and the choice of autocorrelation function to form A determines the covariance kernel of the resulting fields. Whilst this method is simple to employ, it suffers greatly in computational expense when considering larger problems (Tang et al. 2020). Alternatives such as the SPDE approach, Karhunen-Loève expansion, or spectral methods offer cheaper alternatives (Müller et al. 2022; Ricketts et al. 2023b). See Ricketts et al. (2023a) for a summary of methods as well as their computational complexity.

The approach for generating periodic random fields is less trivial. Recently, CMD has been employed using a modified squared exponential kernel, enforcing periodicity at opposing boundaries (González Acosta et al. 2023). The periodicity of the autocorrelation function matched the domain width, enforcing the same resulting field values at opposing boundaries. Due to the application, only horizontal periodicity was necessary, but this could be readily extended to all opposing boundaries. In this paper, an approach derived from Hu and Tonder (1992) is employed in generating periodic self-affine surfaces (Yastrebov et al. 2017). The method is based on filtering in the Fourier space of random noise such that a fractal surface is generated, and depending on the cut off frequencies in the Fourier space, the generated surfaces can be made Gaussian in nature. The advantages of having smooth Gaussian fields has already been highlighted, but this approach of variable roughness through the choice of cut-off frequencies allows for roughness to be introduced into the plurigaussian simulation method, leading to more flexibility in representing discrete rough geometries. For further details on the approach, see Yastrebov et al. (2015).

2.2 Numerical Homogenisation

Generally, numerical homogenisation approaches are used to conduct multi-scale analyses where the material response is computed by solving a boundary value problem (BVP) on a representative volume of the microstructure. This can be done for multiple scales, for example, macro- and micro-scales. The first step in this approach is to define a microstructural representative volume element (RVE) that represents the characteristics of the material in terms of its physical geometry. The RVE is used as the domain of the micro-scale BVP, and allows for the calculation of macroscopic quantities through a domain averaging scheme. Here, the RVE is generated through the appropriate use of P-PGS. In the following, the formulation of the thermal problem at both the macro and micro-scale -denoted with M and m respectively- as well as the scheme for micro to macro transition will be given.

The approach taken follows the work of Özdemir et al. (2008), where the principles of numerical homogenisation are extended to thermal problems based on the work of Kouznetsova et al. (2001) for stress analyses. The time dependency of heat storage is neglected at the micro-scale, such that steady-state thermal equilibrium is achieved as

$$\nabla_m \cdot \mathbf{q_m}(\boldsymbol{x}) = 0 \tag{3}$$

where $\mathbf{q}_m(\boldsymbol{x})$ is the microscopic heat flux vector. The solution of (3) over the volume V of the RVE domain requires proper boundary conditions in terms of a prescribed temperature of heat flux normal to the boundary Γ. At the macro-level, heat balance takes the form of

$$\left(\rho c_v\right)_M \dot{\theta}_M + \nabla_M \cdot \mathbf{q_M} = 0 \tag{4}$$

where $\left(\rho c_v\right)_M$ is the heat capacity, θ is the temperature where the $\dot{\theta}$ indicates the time derivative, and $\mathbf{q_M}$ is the macroscopic flux. Again, this balance equation requires macro-level boundary conditions and additional initial conditions for its solution. In this study, numerical homogenisation is used to obtain the macroscopic flux from the solution over the micro-scale RVE. This is done such that the macroscopic effective thermal conductivity can be evaluated. As suggested by Eq. (3), the heat storage is neglected at the micro-scale. The same assumption is made at the macro-level, such that the steady-state solution can be computed. If a multi-level transient simulation was conducted, then this could be upscaled from the micro-level such that the heat capacity is preserved.

Using a multi-scale approach, the microscopic temperature profile $\theta_m(\boldsymbol{x})$ for a position vector $\boldsymbol{x}$ can be decomposed without loss of generality into a spatially linear mean field at the macro-level, and a fluctuation field $\theta_f(\boldsymbol{x})$, where

$$\theta_m(\boldsymbol{x}) = \theta_m^k + \nabla_M \theta_M \cdot \left(\boldsymbol{x} - \boldsymbol{x}^k\right) + \theta_f(\boldsymbol{x}) \tag{5}$$

where θ_m^k is the temperature at an arbitrary point $\boldsymbol{x}^k$ within the RVE (Özdemir et al. 2008). This can be seen as a perturbation of a mean macroscopic field that has fluctuations at the micro-scale due to material property variations in the RVE, in this case being the conductivity.

Heat conduction is driven by the temperature gradient that develops in the domain due to the applied boundary conditions. Thus, temperature gradients should be preserved in the transition between scales. As the temperature field is additively split into its micro and macro contributions as in Eq. (5), the volume averaged micro-scale temperature gradient can be written as

$$\frac{1}{V} \int_V \nabla_m \theta_m \mathrm{d}V = \nabla_M \theta_M + \frac{1}{V} \int_\Gamma \theta_f \boldsymbol{n} \mathrm{d}\Gamma \tag{6}$$

where the Gauss divergence theorem is applied to the volume integral involving the fluctuation field to convert it to an integral over Γ, the domain boundary, and $\nabla_M \theta_M$ is the gradient reflecting the thermal effects of macroscopic heat flow transferred through the boundary conditions to the RVE. The introduction of a scale transition to enforce the macroscopic temperature gradient to equal the volume average of its microscopic counterpart leads to the constraint

$$\int_\Gamma \theta_f \boldsymbol{n} \mathrm{d}\Gamma = 0 \tag{7}$$

and is satisfied by RVE boundary conditions to be defined.

The scale transition constraint (7) can be explicitly written as

$$\int_{\Gamma^L} \left\{ \theta_{\mathrm{f}}^L - \theta_{\mathrm{f}}^R \right\} \boldsymbol{n}^L \mathrm{d}\Gamma + \int_{\Gamma^B} \left\{ \theta_{\mathrm{f}}^B - \theta_{\mathrm{f}}^T \right\} \boldsymbol{n}^B \mathrm{d}\Gamma = 0 \tag{8}$$

where L, R, B, T, represent the left, right, bottom and top boundaries of the microscopic RVE.

For Eqs. (7) and (8) to be true, the fluctuation field θ_{f} must equal zero. Thus, the fluctuation field is neglected from Eq. (5), and the macro and microscopic quantities can be formulated as

$$\theta_{\mathrm{m}}^R - \theta_{\mathrm{m}}^L = \nabla_{\mathrm{M}} \theta_{\mathrm{M}} \cdot \left(\boldsymbol{x}^R - \boldsymbol{x}^L \right) \tag{9}$$

and

$$\theta_{\mathrm{m}}^T - \theta_{\mathrm{m}}^B = \nabla_{\mathrm{M}} \theta_{\mathrm{M}} \cdot \left(\boldsymbol{x}^T - \boldsymbol{x}^B \right) \tag{10}$$

These relate to periodic boundary conditions which naturally enforce anti-periodic normal flux at the boundary due to the heat balance equation. It is noted that the use of periodic boundary conditions is purely mathematically motivated and does not imply geometric restrictions on the micro-scale domain. Their application has been seen to give better predictions when applied as opposed to uniform boundary conditions (Hazanov and Huet 1994; Hori and Nemat-Nasser 1999; Bouaoune et al. 2016; Tian et al. 2019).

The micro–macro scale transition can be achieved by first considering the second law of thermodynamics, which then leads to Fourier's inequality

$$-\frac{1}{\theta} \nabla \theta \cdot \mathbf{q} \geq 0 \tag{11}$$

being the entropy change due to heat conduction. Eliminating θ from the denominator and enforcing consistent entropy change at both the macro- and micro-level results in

$$\frac{1}{V} \int_V \nabla_{\mathrm{m}} \theta_{\mathrm{m}} \cdot \mathbf{q}_{\mathrm{m}} \mathrm{d}V = \nabla_{\mathrm{M}} \theta_{\mathrm{M}} \cdot \mathbf{q}_{\mathrm{M}} \tag{12}$$

implying that the change in entropy due to heat conduction at the macro-level should be consistent with that at the micro-level. Thus, from Eqs. (6) and (7), the micro and macro flux fields can be associated through

$$\frac{1}{V} \int_V \mathbf{q}_{\mathrm{m}} \mathrm{d}V = \mathbf{q}_{\mathrm{M}} \tag{13}$$

showing that the volume averaged micro-scale heat flux is equivalent to the macroscopic heat flux.

3 Numerical Formulation

In the following, the numerical approach to solving the thermal problem at the micro-scale is presented, as well as details relating to the implementation of the P-PGS framework.

3.1 Finite Element Framework: Thermal Diffusion

As previously stated, numerical homogenisation is employed to calculate the effective thermal properties at the pore-scale of cement paste, specifically to attain the effective thermal conductivity of the medium. This is done through solving a BVP with appropriate boundary conditions and constitutive components over the RVE using the FEM. Before the solution process begins, the microstructures generated through P-PGS are read in as an image, and used to define material sub-domains that can be assigned distinct material properties, in this case being the different thermal conductivities of the medium.

The transfer of heat at the micro-scale is governed by nothing more than a description of diffusion governed by Poisson's equation. There are many approaches to solving this, but here the standard variational form of the steady-state Poisson's equation is employed and solved in FEniCS over the RVE (Logg et al. 2012). Periodic boundary conditions akin to those given in Eqs. (9) and (10) are enforced through the function space definition, such that the periodic fluctuation at the micro-scale is solved for directly. Following this, the solution can be averaged over the domain as in Eq. (13) to directly give the effective thermal conductivity of the medium at the macroscale.

The problem is given as

$$
\begin{aligned}
-\nabla \cdot \left(k \left(\nabla \theta_M + \nabla \theta_m \right) \right) &= \text{in } \Omega \\
\theta_m^R - \theta_m^L &= \nabla_M \theta_M \cdot \left(x^R - x^L \right) \text{on } \Gamma_{LR} = \Gamma_L \cup \Gamma_R \\
\theta_m^T - \theta_m^B &= \nabla_M \theta_M \cdot \left(x^T - x^B \right) \text{ on } \Gamma_{TB} = \Gamma_T \cup \Gamma_B
\end{aligned}
\tag{14}
$$

where $\Omega \in \mathbb{R}^2$ is the problem domain whose boundary $\partial\Omega$ has periodic boundary conditions enforced between opposing boundaries, k is the thermal conductivity, and θ_m is the periodic fluctuation in Ω. To compute the effective thermal conductivity k, Fourier's law $k \cdot \nabla \theta_M = \mathbf{q}_M$ is employed, where $\mathbf{q}_M$ is the macroscopic flux computed by taking the volume-average of the microscopic flux see Eq. 13 and $\nabla \theta_M$ is the prescribed macroscopic temperature gradient as in Eq. (14).

The domain is discretised into linear Lagrangian triangular elements in a uniform grid, and can be posed as: find $\theta_m \in H^1(\Omega)$ such that

$$
\int_\Omega \nabla \hat{\theta}_m k \cdot \left(\nabla \theta_M + \nabla \theta_m \right) d\Omega = \int_\Omega \hat{\theta}_m f d\Omega, \ \forall \hat{\theta}_m \in H^1(\Omega)
\tag{15}
$$

where $\hat{\theta}_m$ are the test functions. This is an ill-posed problem, so an additional constraint of zero-average of the fluctional field θ_m is applied through additional Lagrange multipliers λ. The problem is then: find $\left(\theta_m, \lambda \right) \in H^1(\Omega) \times \mathbb{R}^2$ such that

$$
\int_\Omega \nabla \hat{\theta}_m k \cdot \left(\nabla \theta_M + \nabla \theta_m \right) d\Omega + \int_\Omega \lambda \cdot \hat{\theta}_m d\Omega + \int_\Omega \hat{\lambda} \cdot \theta_m d\Omega = \int_\Omega \hat{\theta}_m f d\Omega
\tag{16}
$$

$\forall \left(\hat{\theta}_m, \hat{\lambda} \right) \in H^1(\Omega) \times \mathbb{R}^2$. This can then be solved numerically by employing the Galerkin weighted residual approach for spatial discretisation. The conductivity tensor is employed in the weak form to represent the differing thermal conductivities of the sub-domains present in the generated microstructures. The domain is discretised such that each pixel contains two linear Lagrangian elements. A schematic to describe the overall process from is presented in Fig. 3, illustration the collection of material
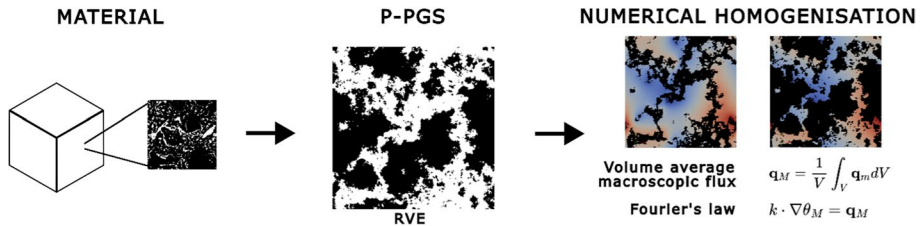
Fig. 3 Schematic of the process for computing the effective thermal conductivity of a given material (part of which is reused with permission after Lyu et al. 2019)

microstructural information, its representation using P-PGS, and the numerical homogenisation that occurs to compute the effective thermal conductivity.

It is noted that the contribution of convective heat transport is neglected in the boundary value problem. As the finite element method is flexible, other physical processes such as convection can be accounted for by including additional terms in the governing equations, and subsequent integrals in the weak form.

3.2 Field Generation

The PGS framework that was mentioned in Ricketts et al. (2023a, b, c) was extended to include the generation of periodic Gaussian random fields. A lithotype rule must first be defined, composed of facies of a given shape. In two dimensions, two periodic Gaussian random fields are generated to convolutionally map each position in the simulation domain to the lithotype rule to determined its phase. This pixel-wise evaluation is saved as an image to be read by the finite element model upon execution. For more details on the effects of lithotype facies, see Ricketts et al. (2023a, b, c).

4 Example Problem: Effective Thermal Properties of Mortar Paste

To assess the applicability of P-PGS in representing material microstructures, the effective thermal conductivity of cement paste was calculated based on the presented numerical homogenisation regime. Experimental measurements from the literature were collected to compare with the calculated values. Specifically data presented by Stolarska and Strzałkowski (2020) of the thermal parameters of mortars based on different water content (W/C) ratios and cement types, namely CEM I 42.5R, CEM II A-S 52.5N and CEM III A 42.5N are considered. Three samples at W/C ratios of 0.5, 0.55, and 0.6 were made for three different cement types with dimensions $25 \times 25 \times 6$ cm. For each of the 9 samples, the thermal conductivity, volume-specific heat and thermal difussivity were analysed under different levels of saturation. Measurements from three consistent points on each sample were taken, such that all samples were measured a total of 9 times, with the mean value of each of the material properties for each sample being reported. The porosity was also evaluated through mercury intrusion porosimetry on two subsamples of each of the 9 samples, with dimensions $0.7 \times 0.7 \times 2$ cm. Table 1 shows a summary of the measured results in terms of their total porosity and average thermal conductivity for each sample. These will be used directly to compare with the calculated equivalents.

Table 1 Summary of measured values of total porosity and average thermal conductivity (after Stolarska and Strzałkowski 2020)

	Sample								
	1	2	3	4	5	6	7	8	9
Cement type	42.5N	42.5N	42.5N	42.5R	42.5R	42.5R	52.5N	52.5N	52.5N
W/C	0.5	0.55	0.6	0.5	0.55	0.6	0.5	0.55	0.6
Porosity (%)	14.28	15.25	16.97	15.92	16.87	17.8	15.94	16.36	16.97
Thermal conductivity of air filled pores (W/mK)	1.67	1.59	1.55	1.47	1.29	1.36	1.38	1.27	1.23
Thermal conductivity of water filled pores (W/mK)	2.42	2.46	2.49	2.53	2.42	2.54	2.42	2.35	2.39
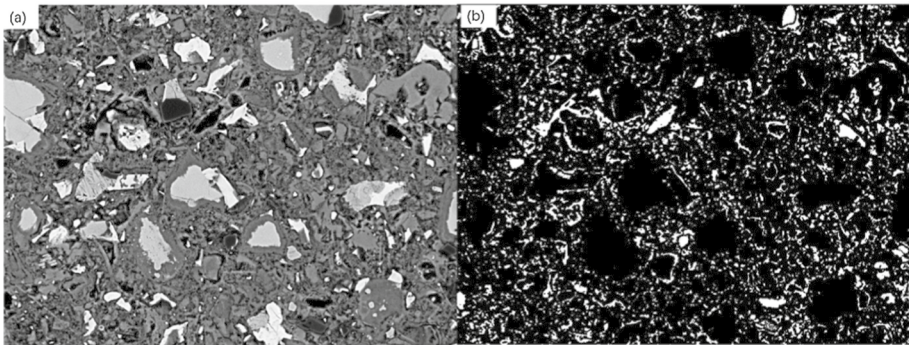
Fig. 4 BSE images of size $190 \times 140\,\mu m$ for cement paste with a W/C ratio of 0.35 for **a** original image and **b** binary image. (reused with permission after Lyu et al. 2019)
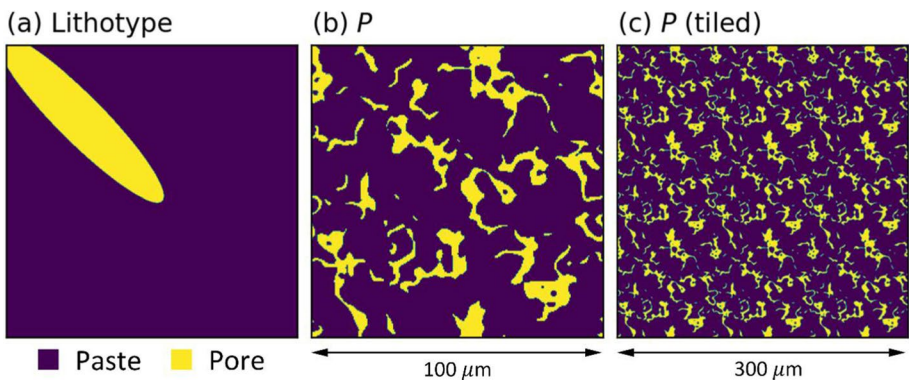
Fig. 5 Illustration of **a** the employed lithotype, **b** generated pore-structure, and **c** is the tiled version to highlight the periodicity

Whilst direct comparison of effective properties is possible, the geometric structure of the samples was not reported, making it challenging to represent through P-PGS. Due to this, the generated microstructures were based upon backscattered electron scanning electron microscope (SEM-BSE) images reported in Lyu et al. (2019) and seen in Fig. 4, where (a) is the raw image and (b) is the binarised equivalent.

The covariance structure of the random fields as well as the lithotype rule used in P-PGS were chosen such that the porosity of the resulting fields matched well with the reported measurements in Table 1, as well as adhering to the geometry seen in Fig. 4. The selected lithotype appears as an off-centre and rotated ellipse, as illustrated in Fig. 5a. Ricketts et al. (2023a, b, c) observed that a central ellipse was an appropriate choice for generating cement paste pore-structures. In this case, the microstructures are less interconnected, and iterative testing suggested that shifting the ellipse from the lithotype's centre encouraged more disconnected structures in the final field. The domain size was chosen to be $100 \times 100\,\mu m$, where a sample realisation can be seen in Fig. 5b.

The periodicity is also highlighted in Fig. 5c, showing the connectivity between opposing boundaries. The low connectivity of the pore-structures is a result of the low porosities seen in Table 1. It has been shown that a porosity of 20% is a sufficient percolation threshold for good predictions of diffusivity in samples of W/C 0.3–0.5 (Patel et al. 2018b). This assumes a certain level of connectivity to allow for percolation, and as the generated porosities are below this threshold, it is fair to assume that they will be made up of larger disconnected pore structures. This is further suggetsed by Fig. 5b. To assess whether the generated microstructures are RVEs, the RVE size was calculated using the open-source image analysis python package PoreSpy (Gostick et al. 2019), where the domain will constitute an RVE once the quatity being analysed changes negligably with increasing domain size. As seen in Fig. 6 for a given generated structure, the porosity converges to a stable value, suggesting that the domain size used is suffient in representing the overall behaviour of the microstructure. It is worth noting that whilst the domain represents an RVE for porsitiy at this scale, this may not be true for other quantities of interest, but this was not determined.

In total, 250 microstructures of size $100 \times 100\,\mu m$ were generated based on the reasoning above. For additional verification of the generated microstructures, their maximal
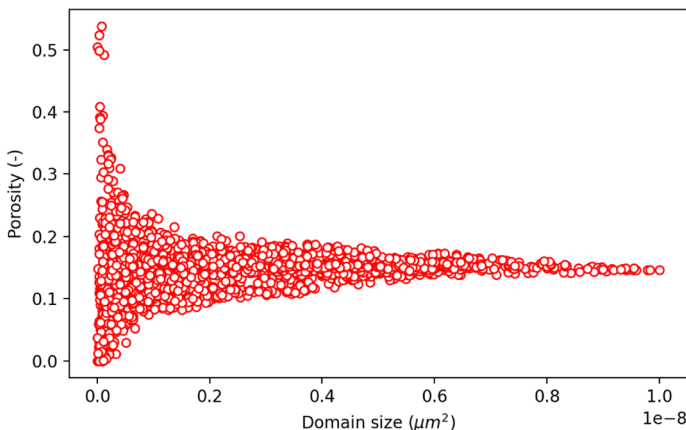

Fig. 6 RVE analysis of a generated pore-structure at $100 \times 100\,\mu m$ highlighting convergence and that the RVE size is suitable
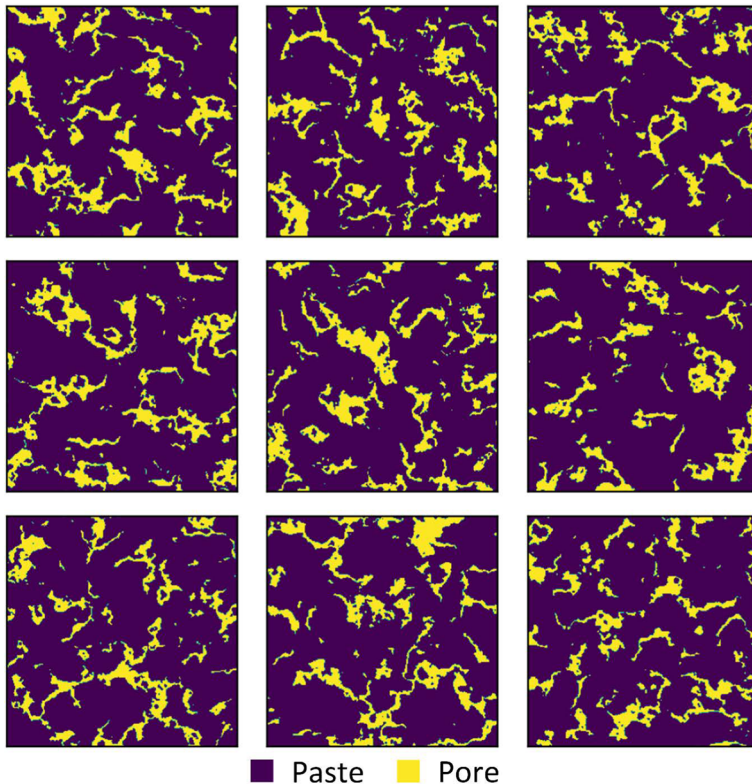
Fig. 7 Samples of generated periodic pore-scale microstructures

pore-size was calculated and compared with experimental results. The calculation is based on assigning each pixel to be the value of the largest circle that overlaps it inside the pore, and was evaluated using PoreSpy (Gostick et al. 2019). This has been reported in the literature as ≤9.47 µm for W/C ratio of 0.3 (Lyu et al. 2019). Due to the stochasticity of the microstructural generation, around 10% of the resulting fields lay outside of the experimental range and were neglected. Similarly, the resulting volume fractions of the microstructures can vary. Those outside of the experimental porosity range of Table 1 (14–18%) were filtered out, leaving 152 images (see Fig. 7 for more examples). It is noted that even with further trial and error through changing the lithotype and input field parameters, the random nature of the approach means that it is often the case that some generated fields will be unsuitable. With such a constrained lithotype as in Fig. 5c, this is inevitable.

The diffusion of heat through the medium was simulated using the approach presented in Sect. 3.1, where material conductivities for the paste and pore phases were taken from the literature. The thermal conductivity of cement paste has been reported in the range of $2.48 \rightarrow 3.43$ W/mK for a porosity of $22.9 \rightarrow 24.10\%$ (Khan 2002). Similarly, the thermal conductivity of air filled pores and water filled pores has been reported as 0.026 and 0.607 W/mK respectively (Liu et al. 2020). The pore-space conductivities are taken directly as model input parameters depending on whether air or water filled pore conditions are being simulated. Here, the porosity of the generated microstructures is lower than

Table 2 Material parameters

	Paste	Air filled pores	Water filled pores
Thermal conductivity (W/mK)	3.43	0.026	0.607
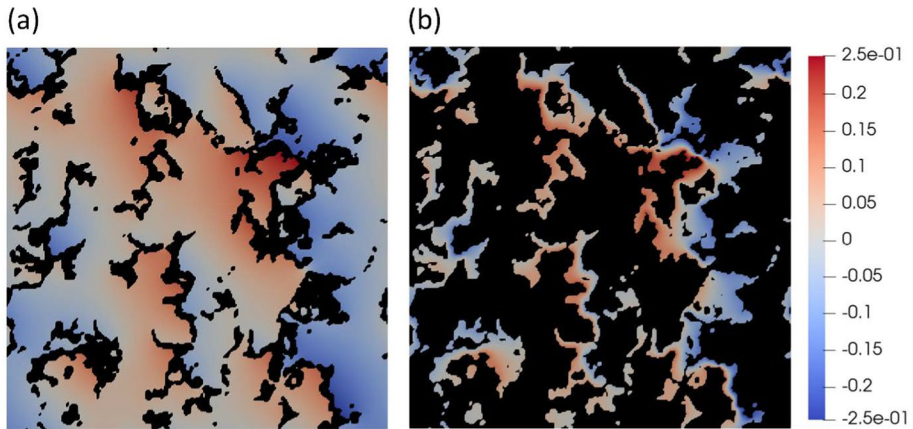
Fig. 8 Microscopic solution of the microscale boundary value problem over **a** the cement paste and **b** the pore-space under air filled conditions
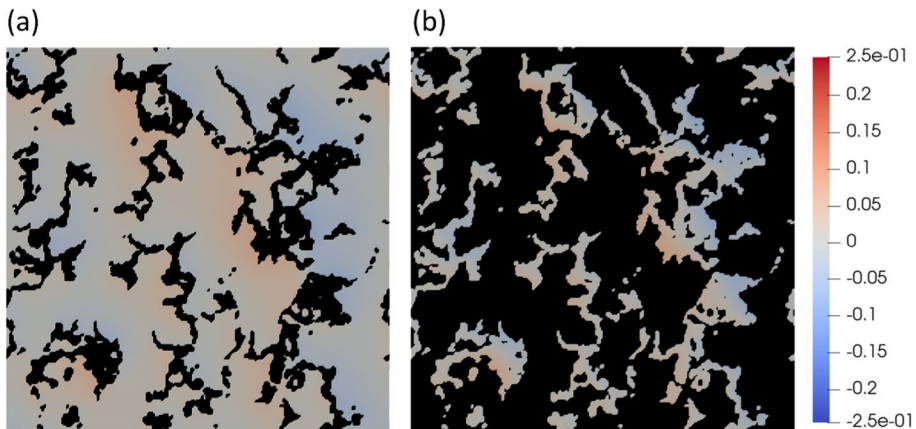
Fig. 9 Microscopic solution of the microscale boundary value problem over **a** the cement paste and **b** the pore-space under water filled conditions

porosity of the samples used to back calculate the reported thermal conductivity associated with the cement paste (Khan 2002), where the authors used Campbell-Allen and Thorne's approach (Campbell-Allen and Thorne 1963). Similarly, it is assumed that the conductivity does not change between cement type, where in reality this could be the case. The material parameters of each phase used in the model are given in Table 2.

Table 3 Comparison of the experimental and calculated thermal conductivity for both air and water filled conditions

	Type	Mean (W/mK)	Relative error (%)	Maximum (W/mK)	Minimum (W/mK)
Air filled pores	Experimental	1.45	–	1.67	1.23
	Numerical	1.43	1.38	1.89	0.85
Water filled pores	Experimental	2.45	–	2.54	2.35
	Numerical	2.44	0.41	2.59	2.27

Figures 8 and 9 show the microscopic solution θ_m over Ω for a given generated microstructure under the assumption of air and water filled pores respectively.

Table 3 shows the comparison between the experimental and numerical results of the effective thermal conductivities for both air and water filled conditions in terms of the mean, maximum and minimum thermal conductivities of all samples.

It can be seen that the calculated mean values match well with the experimental observations for both conditions, suggesting that the generated microstructures are representative of these materials in terms of their geometry. A greater range of calculated thermal conductivities is seen numerically when compared with the experimental observations. Clearly, the evaluation of many more samples of varied porosities and pore structures will widen the range in which the calculated conductivities will lie. This enlarged range is most pronounced in the case of air filled pores, as seen in Fig. 10, due to the much larger ratio between the conductivity of the paste and pore phases.

The structure of the pores -as well as the overall porosity- will have a greater effect on the diffusive process, leading to more variability in the calculated effective properties as is seen in Table 3. Similarly, the maximum and minimum experimental values given in Table 3 are in fact the maximum and minimum of the mean samples values that were reported in Stolarska and Strzałkowski (2020). As the authors did not report the variability in the measurements of each sample, it is likely that the true maximum and minimum would differ from the given values.
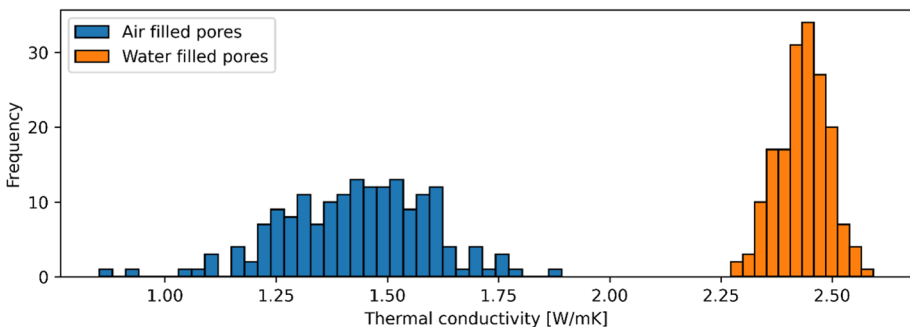
Fig. 10 Histograms of the calculated thermal conductivities

5 Concluding Remarks

An extension of the plurigaussian simulation method has been presented, such that the generated structures are periodic in nature. The use of periodic random fields ensures periodicity in the resulting structures, a characteristic that is particularly important when calculating effective material properties. Heat diffusion was simulated at the pore-scale of cement paste, and numerical homogenisation employed to calculate its effective thermal conductivity. This was done to assess how representative the generated microstructures are of the pore-scale geometry. Strong agreement was obtained between the numerical and experimental observations, suggesting that P-PGS is appropriate for generating complex material microstructures. Using such an approach mitigates the reliance on empirical formulas and experimental calibration, reducing the cost and time associated with material testing or design. This computationally inexpensive method can generate complex structures in a stochastic manner, and is appropriate for material representation at all scales.

When considering a given material at different scales, numerous phases could be present. The presented approach is not limited to two phase materials as seen here, both in the microstructure or heat diffusion stage for computational homogenisation. P-PGS allows for an arbitrary number of phases to be represented by choosing a lithotype rule that contains information about all phases present in the material at a given scale, making it suitable for a wide range of material microstructures. The difficulty lies in choosing an appropriate lithotype as a given microstructure can be generated through many morphologically equivalent lithotypes. Investigation into this matter is on-going. The approach is also extendable to 3-D, where the calculated effective properties would be more sensitive to the complex pore geometries. Similarly, other processes could be modelled such as electrical diffusion and its associated properties, as well as transient solutions at differing scales.

Many approaches to numerical homogenisation or simulation over RVE BVPs employ idealised representations of the material geometry. Whilst for many cases this can be appropriate, the use of discrete geometrically consistent representations can lead to more accurate estimations of effective material properties and is something that P-PGS can provide.

Data Availability Information on the data underpinning the results presented here, including how to access them, can be found in the Cardiff University data catalogue at (https://doi.org/10.17035/d.2023.02838 12950).

Declarations

Conflict of interest The authors declare no competing interests.

References

Abdallah, B., Willot, F., Jeulin, D.: Morphological modelling of three-phase microstructures of anode layers using SEM images. J. Microsc. **263**(1), 51–63 (2016). https://doi.org/10.1111/jmi.12374

Andreassen, E., Andreasen, C.S.: How to determine composite material properties using numerical homogenization. Comput. Mater. Sci. **83**, 488–495 (2014). https://doi.org/10.1016/j.commatsci.2013.09.006

Armstrong, M., et al.: Plurigaussian Simulations in Geosciences. Berlin Springer, Berlin (2014)

Auriault, J.L.: Effective macroscopic description for heat conduction in periodic composites. Int. J. Heat Mass Transf. **26**(6), 861–869 (1983). https://doi.org/10.1016/S0017-9310(83)80110-0

Bentz, D.P.: Quantitative comparison of real and CEMHYD3D model microstructures using correlation functions. Cem. Concr. Res. **36**(2), 259–263 (2006). https://doi.org/10.1016/j.cemconres.2005.07.003

Betzhold, J., Roth, C.: Characterizing the mineralogical variability of a Chilean copper deposit using plurigaussian simulations. J. s. Afr. Inst. Min. Metall. **100**(2), 111–120 (2000)

Beucher, H., Renard, D.: Truncated Gaussian and derived methods. C.R. Geosci. **348**(7), 510–519 (2016). https://doi.org/10.1016/j.crte.2015.10.004

Bindal, A., Ierapetritou, M.G., Balakrishnan, S., Armaou, A., Makeev, A.G., Kevrekidis, I.G.: Equation-free, coarse-grained computational optimization using timesteppers. Chem. Eng. Sci. **61**(2), 779–793 (2006). https://doi.org/10.1016/j.ces.2005.06.034

Bouaoune, L., Brunet, Y., El Moumen, A., Kanit, T., Mazouz, H.: Random versus periodic microstructures for elasticity of fibers reinforced composites. Compos. B Eng. **103**, 68–73 (2016). https://doi.org/10.1016/j.compositesb.2016.08.026

Campbell-Allen, D., Thorne, C.P.: The thermal conductivity of concrete. Mag. Concr. Res. **15**(43), 39–48 (1963). https://doi.org/10.1680/macr.1963.15.43.39

Chaturantabut, S., Sorensen, D.C.: Nonlinear model reduction via discrete empirical interpolation. SIAM J. Sci. Comput. **32**(5), 2737–2764 (2010). https://doi.org/10.1137/090766498

Chautru, J.M., Meunier, R., Binet, H., Bourges, M.: Geobodies stochastic analysis for geological model parameter inference. Pet. Geostat. **23**, 293–297 (2015). https://doi.org/10.3997/2214-4609.201413643

Cruz, D., Talbert, D.A., Eberle, W. and Biernacki, J. A neural network approach for predicting microstructure development in cement. In: Proceedings of the 2016 International Conference on Artificial Intelligence. pp. 328–334. (2016)

Doligez, B., Hamon, Y., Barbier, M., Nader, F., Lerat, O. and Beucher, H. Advanced workflows for joint modelling of sedimentary facies and diagenetic overprint, impact on reservoir quality. In: All Days. SPE. https://onepetro.org/SPEATCE/proceedings/11ATCE/All-11ATCE/Denver,%20Colorado,%20USA/148514 (2011)

Dowd, P.A., Pardo-Igúzquiza, E., Xu, C.: Plurigau: a computer program for simulating spatial facies using the truncated plurigaussian method. Comput. Geosci. **29**(2), 123–141 (2003). https://doi.org/10.1016/s0098-3004(02)00070-5

Evans, A.G.: Microfracture from thermal expansion anisotropy—I single phase systems. Acta Metall. **26**(12), 1845–1853 (1978). https://doi.org/10.1016/0001-6160(78)90097-4

Feyel, F., Chaboche, J.-L.: FE2 multiscale approach for modelling the elastoviscoplastic behaviour of long fibre SiC/Ti composite materials. Comput. Methods Appl. Mech. Eng. **183**(3–4), 309–330 (2000). https://doi.org/10.1016/S0045-7825(99)00224-8

Galli, A., Beucher, H., le Loc'h, G., Doligez, B., Group, H.: The pros and cons of the truncated Gaussian method. Geostat. Simul. (1994). https://doi.org/10.1007/978-94-015-8267-4_18

Ghavamian, F., Simone, A.: Accelerating multiscale finite element simulations of history-dependent materials using a recurrent neural network. Comput. Methods Appl. Mech. Eng. **357**, 112594 (2019). https://doi.org/10.1016/j.cma.2019.112594

Ghavamian, F., Tiso, P., Simone, A.: POD–DEIM model order reduction for strain-softening viscoplasticity. Comput. Methods Appl. Mech. Eng. **317**, 458–479 (2017). https://doi.org/10.1016/j.cma.2016.11.025

Ghosh, S., Liu, Y.: Voronoi cell finite element model based on micropolar theory of thermoelasticity for heterogeneous materials. Int. J. Numer. Meth. Eng. **38**(8), 1361–1398 (1995). https://doi.org/10.1002/nme.1620380808

Gibiansky, L.V., Torquato, S.: Thermal expansion of isotropic multiphase composites and polycrystals. J. Mech. Phys. Solids **45**(7), 1223–1252 (1997). https://doi.org/10.1016/S0022-5096(96)00129-9

González Acosta, J.L., Varkey, D., Van Den Eijnden, A.P. and Hicks, M.A. Periodic random fields to perform site response and liquefaction susceptibility analysis. In: 10th European Conference on Numerical Methods in Geotechnical Engineering. https://doi.org/10.53243/NUMGE2023-198 (2023)

Gostick, J., Khan, Z., Tranter, T., Kok, M., Agnaou, M., Sadeghi, M., Jervis, R.: PoreSpy: a python toolkit for quantitative analysis of porous media images. J. Open Sour. Softw. **4**(37), 1296 (2019). https://doi.org/10.21105/joss.01296

Goury, O., Amsallem, D., Bordas, S.P.A., Liu, W.K., Kerfriden, P.: Automatised selection of load paths to construct reduced-order models in computational damage micromechanics: from dissipation-driven random selection to Bayesian optimization. Comput. Mech. **58**(2), 213–234 (2016). https://doi.org/10.1007/s00466-016-1290-2

Hashin, Z.: Analysis of composite materials—A Survey. J. Appl. Mech. **50**(3), 481–505 (1983). https://doi.org/10.1115/1.3167081

Hazanov, S., Huet, C.: Order relationships for boundary conditions effect in heterogeneous bodies smaller than the representative volume. J. Mech. Phys. Solids **42**(12), 1995–2011 (1994). https://doi.org/10.1016/0022-5096(94)90022-1

Holla, V., Vu, G., Timothy, J.J., Diewald, F., Gehlen, C., Meschke, G.: Computational generation of virtual concrete mesostructures. Materials **14**(14), 3782 (2021). https://doi.org/10.3390/ma14143782

Hori, M., Nemat-Nasser, S.: On two micromechanics theories for determining micro–macro relations in heterogeneous solids. Mech. Mater. **31**(10), 667–682 (1999). https://doi.org/10.1016/S0167-6636(99)00020-4

Hu, Y.Z., Tonder, K.: Simulation of 3-D random rough surface by 2-D digital filter and fourier analysis. Int. J. Mach. Tools Manuf **32**(1–2), 83–90 (1992). https://doi.org/10.1016/0890-6955(92)90064-N

Jiang, M., Jasiuk, I., Ostoja-Starzewski, M.: Apparent thermal conductivity of periodic two-dimensional composites. Comput. Mater. Sci. **25**(3), 329–338 (2002). https://doi.org/10.1016/S0927-0256(02)00234-3

Kerfriden, P., Gosselet, P., Adhikari, S., Bordas, S.P.A.: Bridging proper orthogonal decomposition methods and augmented Newton-Krylov algorithms: an adaptive model order reduction for highly nonlinear mechanical problems. Comput. Methods Appl. Mech. Eng. **200**(5–8), 850–866 (2011). https://doi.org/10.1016/j.cma.2010.10.009

Khan, M.I.: Factors affecting the thermal properties of concrete and applicability of its prediction models. Build. Environ. **37**(6), 607–614 (2002)

Kouznetsova, V., Brekelmans, W.A.M., Baaijens, F.P.T.: An approach to micro-macro modeling of heterogeneous materials. Comput. Mech. **27**(1), 37–48 (2001). https://doi.org/10.1007/s004660000212

Le Houx, J., Ruiz, S., McKay Fletcher, D., Ahmed, S., Roose, T.: Statistical effective diffusivity estimation in porous media using an integrated on-site imaging workflow for synchrotron users. Transp. Porous Media (2023). https://doi.org/10.1007/s11242-023-01993-7

le Loc'h, G., Galli, A.: Truncated plurigaussian method: theoretical and practical points of view. Geostat. wollongong **96**, 211–222 (1997)

Lefik, M., Boso, D.P., Schrefler, B.A.: Artificial neural networks in numerical modelling of composites. Comput. Methods Appl. Mech. Eng. **198**(21–26), 1785–1804 (2009). https://doi.org/10.1016/j.cma.2008.12.036

Li, D.Q., Xiao, T., Zhang, L.M., Cao, Z.J.: Stepwise covariance matrix decomposition for efficient simulation of multivariate large-scale three-dimensional random fields. Appl. Math. Model. **68**, 169–181 (2019). https://doi.org/10.1016/j.apm.2018.11.011

Liu, C., Qian, R., Liu, Z., Liu, G., Zhang, Y.: Multi-scale modelling of thermal conductivity of phase change material/recycled cement paste incorporated cement-based composite material. Mater. Des. **191**, 108646 (2020). https://doi.org/10.1016/j.matdes.2020.108646

Logg, A., Mardal, K.-A. Wells, G.: (eds.) Automated solution of differential equations by the finite element method. Springer, Berlin Heidelberg (2012). https://doi.org/10.1007/978-3-642-23099-8

Lyu, K., She, W., Miao, C., Chang, H., Gu, Y.: Quantitative characterization of pore morphology in hardened cement paste via SEM-BSE image analysis. Constr. Build. Mater. **202**, 589–602 (2019). https://doi.org/10.1016/j.conbuildmat.2019.01.055

Madani, N., Biranvand, B., Naderi, A., Keshavarz, N.: Lithofacies uncertainty modeling in a siliciclastic reservoir setting by incorporating geological contacts and seismic information. J. Pet. Explor. Prod. Technol. **9**(1), 1–16 (2018). https://doi.org/10.1007/s13202-018-0531-7

Maleki, M., Emery, X.: Joint simulation of grade and rock type in a stratabound copper deposit. Math. Geosci. **47**(4), 471–495 (2014). https://doi.org/10.1007/s11004-014-9556-8

Martinius, A.W., Fustic, M., Garner, D.L., Jablonski, B.V.J., Strobl, R.S., MacEachern, J.A., Dashtgard, S.E.: Reservoir characterization and multiscale heterogeneity modeling of inclined heterolithic strata for bitumen-production forecasting, McMurray formation, Corner, Alberta, Canada. Mar. Pet. Geol. **82**, 336–361 (2017). https://doi.org/10.1016/j.marpetgeo.2017.02.003

Matheron, G., Beucher, H., de Fouquet, C., Galli, A., Guerillot, D., Ravenne, C.: Conditional simulation of the geometry of fluvio-deltaic reservoirs. SPE **16753**, 123–131 (1987). https://doi.org/10.2118/16753-ms

Méndez-Venegas, J., Díaz-Viera, M.A.: Geostatistical modeling of clay spatial distribution in siliciclastic rock samples using the plurigaussian simulation method. Geofísica Internacional **52**(3), 229–247 (2013). https://doi.org/10.1016/S0016-7169(13)71474-0

Mery, N., Emery, X., Cáceres, A., Ribeiro, D., Cunha, E.: Geostatistical modeling of the geological uncertainty in an iron ore deposit. Ore Geol. Rev. **88**, 336–351 (2017). https://doi.org/10.1016/j.oregeorev.2017.05.011

Müller, S., Schüler, L., Zech, A., Heße, F.: GSTools v1.3: a toolbox for geostatistical modelling in python. Geosci. Model Develop. **15**(7), 3161–3182 (2022)

Noor, A.K., Shah, R.S.: Effective thermoelastic and thermal properties of unidirectional fiber-reinforced composites and their sensitivity coefficients. Compos. Struct. **26**(1–2), 7–23 (1993). https://doi.org/10.1016/0263-8223(93)90040-W

Özdemir, I., Brekelmans, W.A.M., Geers, M.G.D.: Computational homogenization for heat conduction in heterogeneous solids. Int. J. Numer. Meth. Eng. **73**(2), 185–204 (2008). https://doi.org/10.1002/nme.2068

Patel, R.A., Perko, J., Jacques, D., De Schutter, G., Ye, G., Van Breugel, K.: A three-dimensional lattice Boltzmann method based reactive transport model to simulate changes in cement paste microstructure due to calcium leaching. Constr. Build. Mater. **166**, 158–170 (2018a). https://doi.org/10.1016/j.conbuildmat.2018.01.114

Patel, R.A., Perko, J., Jacques, D., De Schutter, G., Ye, G., Van Bruegel, K.: Effective diffusivity of cement pastes from virtual microstructures: role of gel porosity and capillary pore percolation. Constr. Build. Mater. **165**, 833–845 (2018b). https://doi.org/10.1016/j.conbuildmat.2018.01.010

Renard, D., Beucher, H.: 3D representations of a uranium roll-front deposit. Appl. Earth Sci. **121**(2), 84–88 (2012). https://doi.org/10.1179/1743275812y.0000000011

Ricketts, E.J., Cleall, P.J., Jefferson, A., Kerfriden, P., Lyons, P.: Representation of three-dimensional unsaturated flow in heterogeneous soil through tractable Gaussian random fields. Géotechnique (2023). https://doi.org/10.1680/jgeot.22.00316

Ricketts, E.J., Cleall, P.J., Jefferson, T., Kerfriden, P., Lyons, P.: Near-boundary error reduction with an optimized weighted Dirichlet-Neumann boundary condition for stochastic PDE-based Gaussian random field generators. Eng. Comput. (2023b). https://doi.org/10.1007/s00366-023-01819-6

Ricketts, E.J., Freeman, B.L., Cleall, P.J., Jefferson, A., Kerfriden, P.: A statistical finite element method integrating a plurigaussian random field generator for multi-scale modelling of solute transport in concrete. Transp. Porous Media (2023c). https://doi.org/10.1007/s11242-023-01930-8

Rocha, I.B.C.M., Kerfriden, P., van der Meer, F.P.: Micromechanics-based surrogate models for the response of composites: a critical comparison between a classical mesoscale constitutive model, hyper-reduction and neural networks. Eur. J. Mech. a. Solids **82**, 103995 (2020). https://doi.org/10.1016/j.euromechsol.2020.103995

Rocha, I.B.C.M., Kerfriden, P., van der Meer, F.P.: On-the-fly construction of surrogate constitutive models for concurrent multiscale mechanical analysis through probabilistic machine learning. J. Comput. Phys. X **9**, 100083 (2021). https://doi.org/10.1016/j.jcpx.2020.100083

Rosen, B.W., Hashin, Z.: Effective thermal expansion coefficients and specific heats of composite materials. Int. J. Eng. Sci. **8**(2), 157–173 (1970). https://doi.org/10.1016/0020-7225(70)90066-2

Stolarska, A., Strzałkowski, J.: The thermal parameters of mortars based on different cement type and W/C ratios. Materials **13**(19), 4258 (2020). https://doi.org/10.3390/ma13194258

Talebi, H., Asghari, O., Emery, X.: Application of plurigaussian simulation to delineate the layout of alteration domains in sungun copper deposit. Open Geosci. **5**(4), 514–522 (2013). https://doi.org/10.2478/s13533-012-0146-3

Tang, K., Wang, J., Li, L.: A prediction method based on Monte Carlo simulations for finite element analysis of soil medium considering spatial variability in soil parameters. Adv. Mater. Sci. Eng (2020). https://doi.org/10.1155/2020/7064640

Teichmann, J., Menzel, P., Heinig, T., van den Boogaart, K.G.: Modeling and fitting of three-dimensional mineral microstructures by multinary random fields. Math. Geosci. **53**(5), 877–904 (2021). https://doi.org/10.1007/s11004-020-09871-4

Teles, V., et al.: Modelling the coupled heterogeneities of the lacustrine microbialite-bearing carbonate reservoir of the yacoraite formation (salta, argentina). Comptes Rendus. Géosci. **355**(S1), 1–20 (2023). https://doi.org/10.5802/crgeos.187

Thilakarathna, P.S.M., Kristombu Baduge, K.S., Mendis, P., Vimonsatit, V., Lee, H.: Mesoscale modelling of concrete—A review of geometry generation, placing algorithms, constitutive relations and

applications. Eng. Fract. Mech. **231**, 106974 (2020). https://doi.org/10.1016/j.engfracmech.2020.106974

Tian, W., Qi, L., Chao, X., Liang, J., Fu, M.: Periodic boundary condition and its numerical implementation algorithm for the evaluation of effective mechanical properties of the composites with complicated micro-structures. Compos. B Eng. **162**, 1–10 (2019). https://doi.org/10.1016/j.compositesb.2018.10.053

Tretiak, K., Plumley, M., Calkins, M., Tobias, S.: Efficiency gains of a multi-scale integration method applied to a scale-separated model for rapidly rotating dynamos. Comput. Phys. Commun. **273**, 108253 (2022). https://doi.org/10.1016/j.cpc.2021.108253

van Breugel, K.: Numerical simulation of hydration and microstructural development in hardening cement-based materials (I) theory. Cem. Concr. Res. **25**(2), 319–331 (1995). https://doi.org/10.1016/0008-8846(95)00017-8

Van Marcke, P., Verleye, B., Carmeliet, J., Roose, D., Swennen, R.: An improved pore network model for the computation of the saturated permeability of porous rock. Transp. Porous Media **85**(2), 451–476 (2010). https://doi.org/10.1007/s11242-010-9572-1

Yang, Y., Wang, K., Zhang, L., Sun, H., Zhang, K., Ma, J.: Pore-scale simulation of shale oil flow based on pore network model. Fuel **251**, 683–692 (2019). https://doi.org/10.1016/j.fuel.2019.03.083

Yastrebov, V.A., Anciaux, G., Molinari, J.-F.: From infinitesimal to full contact between rough surfaces: evolution of the contact area. Int. J. Solids Struct. **52**, 83–102 (2015). https://doi.org/10.1016/j.ijsolstr.2014.09.019

Yastrebov, V.A., Anciaux, G., Molinari, J.-F.: The role of the roughness spectral breadth in elastic contact of rough surfaces. J. Mech. Phys. Solids **107**, 469–493 (2017). https://doi.org/10.1016/j.jmps.2017.07.016

Yunsel, T.Y., Ersoy, A.: Geological modeling of gold deposit based on grade domaining using plurigaussian simulation technique. Nat. Resour. Res. **20**(4), 231–249 (2011). https://doi.org/10.1007/s11053-011-9150-4

Zagayevskiy, Y., Deutsch, Cv.: Grid-free petroleum reservoir characterization with truncated pluri-Gaussian simulation: hekla case study. Pet. Geosci. **22**(3), 241–256 (2016). https://doi.org/10.1144/petgeo2015-078

Zhang, J., Wang, Z., Yang, H., Wang, Z., Shu, X.: 3D meso-scale modeling of reinforcement concrete with high volume fraction of randomly distributed aggregates. Constr. Build. Mater. **164**, 350–361 (2018). https://doi.org/10.1016/j.conbuildmat.2017.12.229